UDK 67.017:620.172:620.173.24
Professional article/Strokovni članek

ISSN 1580-2949
MTAEC9, 51(3)549(2017)

# TENSILE BEHAVIOUR AND FRACTOGRAPHY ANALYSES OF LM6/$ZrO_2$ COMPOSITES

## OBNAŠANJE IN ANALIZA PRI NATEZNI OBREMENITVI PRELOMA KOMPOZITOV LM6/$ZrO_2$

**Govindan Karthikeyan[1], Gowthanithankachi Raghuvaran Jinu[2]**

[1]University College of Engineering Pattukottai, A Constituent College of Anna University Chennai, Department of Mechanical Engineering, Rajamadam, Pattukottai-614701, Tamilnadu, India
[2]University College of Engineering, Department of Mechanical Engineering, Nagercoil-629004, Tamilnadu, India
p_gkarthikeyan@yahoo.co.in, gr_jinu1980@yahoo.com

*Prejem rokopisa – received: 2015-10-21; sprejem za objavo – accepted for publication: 2016-06-15*

doi:10.17222/mit.2015.319

Aluminium-based metal matrix (LM6) composite materials were prepared using various percentages of 0 %, 3 %, 6 %, 9 % and 12 % of zirconia by the weight fraction method and fabricated by the stir casting method. Five samples were prepared as per the ASTM B-557-M-94 standard, and then the prepared sample was subjected to an energy-dispersive spectrometry (EDS), hardness and tensile tests. The hardness and tensile test results revealed that the maximum hardness, maximum ultimate strength, yield strength was obtained for the composite containing 12 % of mass fractions of $ZrO_2$. The percentage of increase in zirconia increases the hardness, ultimate strength, yield strength. The minimum percentage of zirconia gives the minimum hardness and ultimate strength. Then EDS test was conducted on prepared samples. It was confirmed that aluminium and zirconia particles are present in the metal matrix composites. Fractography analysis was also employed in this work to understand the fracture mechanics of the surface. The fractography analysis was conducted with a scanning electron microscope (SEM). From the fractography analysis it was revealed that the nature of the fracture surface was changed from ductile with a large dimple surface to brittle fracture.

Keywords: metal matrix composites, aluminium LM6 alloy, zirconia ($ZrO_2$), tensile test, fractography

Kovinski kompoziti na osnovi aluminija (LM6) so bili pripravljeni z različnimi masnimi deleži 0 %, 3 %, 6 %, 9 % in 12 % cirkonijevega dioksida, z metodo ulivanja z mešanjem taline. Pet vzorcev je bilo pripravljenih skladno s standardom ASTM B-557-M-94 in nato pregledanih z energijsko disperzijsko spektrometrijo (EDS), izmerjena je bila trdota in izvedeni so bili natezni preizkusi. Iz meritve trdote in nateznih preizkusov sledi, da je bila največja trdota in najvišja natezna trdnost dosežena pri kompozitu z 12 masnimi % $ZrO_2$. Naraščajoča vsebnost cirkonijevega dioksida povišuje trdoto, natezno trdnost in mejo plastičnosti. Najmanjša vsebnost cirkonijevega dioksida daje najmanjšo trdoto in najnižjo natezno trdnost. Na pripravljenih vzorcih je bila izvedena tudi EDS analiza, ki je potrdila, da sta aluminij in delci iz cirkonijevega dioksida prisotna v kovinski osnovi kompozita. Analiza prelomov je bila tudi uporabljena v tem delu, da bi razumeli mehaniko preloma površine. Analiza prelomov je bila izvedena z vrstičnim elektronskim mikroskopom. Analiza prelomov je odkrila, da se narava površine preloma spreminja iz duktilnega z velikimi jamicami, v krhek prelom.

Ključne besede: kompoziti s kovinsko osnovo, aluminijeva LM6 zlitina, cirkonijev dioksid ($ZrO_2$), natezni preizkus, analiza preloma

## 1 INTRODUCTION

Metal matrix composites offer various advantages in applications where high specific strength, stiffness, and resistance are required.[1] Aluminium-based composites containing ceramic whiskers, fibers and particles have been used for automobile parts such as pistons and cylinder liners in engines due to their superior wear properties.[2] Stir casting techniques are the conventional and economic way of producing AMC. But with the conventional stir casting techniques, it is difficult to produce a particulate reinforced composite.[3] They are usually reinforced by $Al_2O_3$, SiC, C, and in addition $SiO_2$, B, BN, $B_4C$ may also be considered.[4] In this field, aluminium is the most popular matrix for the metal matrix composites. Most of the research works deal with aluminium matrix because of their lightweight nature. The Al alloys are quite attractive due to their low density, good corrosion resistance, processing flexibility, high thermal and electrical conductivity, improved elastic modulus, strength and their high damping capacity. Different processing techniques are used for the production of aluminium metal matrix composites. A lot of researchers have concentrated on developing new composites such as Al 6061, LM25, reinforcing with various elements such as $TiB_2$, SiC, TiC, $ZrB_2$, AIN, $Si_3N_4$, $Al_2O_3$ and their tensile properties were analyzed in earlier researchers.[3-6] Very few works were identified in analyzing the effect of $ZrO_2$ on the tensile behavior. Zirconia is a refractory material with a melting point of about 2680 °C. $ZrO_2$ possesses good properties, such as a low coefficient of thermal expansion, good thermal shock resistance, high melting point, low thermal conductivity and excellent thermal stability. Its density, Young's modulus, and hardness are 5.71 g/cm$^3$, 190 GPa and 1200 HV, respectively.

**Table 1:** Chemical composition of aluminum LM6 alloy, in mass fractions (*w*/%)
**Tabela 1:** Kemijska sestava aluminijeve zlitine LM6 v masnih odstotkih (*w*/%)

| Cu | Mg | Si | Fe | Mn | Ni | Zn | Pb | Sn | Ti | Al |
|---|---|---|---|---|---|---|---|---|---|---|
| 0.1 | 0.10 | 10-13 | 0.6 | 0.5 | 0.1 | 0.1 | 0.1 | 0.05 | 0.2 | Bal |

No works have been identified in analyzing the effect of $ZrO_2$ on LM6 base material while subjected to tensile and fractography analysis. Hence, the works mainly concentrated on developing new composite material by taking LM6 as the base material and varying the percentage of $ZrO_2$ to identify the influence of $ZrO_2$ on the tensile and fracture behavior. The tensile strength and fractography analysis of these materials were also studied. The present research is an attempt to test and analyze the mechanical properties of LM6 reinforced with (0, 3, 6, 9 and 12) % various by weight fractions of $ZrO_2$ particulate produced by the stir casting method.

## 2 MATERIALS AND METHODS

### *2.1 Experimental part*

The LM6 aluminium alloy was taken as the base material and $ZrO_2$ powder (particle size 1–10 μm) was chosen as the reinforcement material. The corresponding chemical compositions are given in **Table 1**. In this work, five cast samples were prepared by keeping LM6 as the base material at varying weight percentage of $ZrO_2$, such as 0 %, 3 %, 6 %, 9 %, and 12 %. The casting was carried out using the stir casting process, as shown in **Figure 1**. Initially, the aluminum LM6 alloy was melted in a pot by heating in a blower furnace at 850 °C for 15 min. The $ZrO_2$ powder was preheated at 575 °C in a separate muffle furnace. The furnace temperature was raised above the liquid temperature of LM 6 at about 850 °C to melt the LM6 completely and then it is slowly added to the preheated $ZrO_2$ powder. The stirring was carried out with the help of the drilling machine for about 15 min and the stirring rate maintained a speed of about 950 $min^{-1}$. This combination was then transferred into the mould cavity, and it is cooled to a room temperature. This procedure was followed for the preparation of five specimens with different compositions of $ZrO_2$ as shown in **Figure 1**.

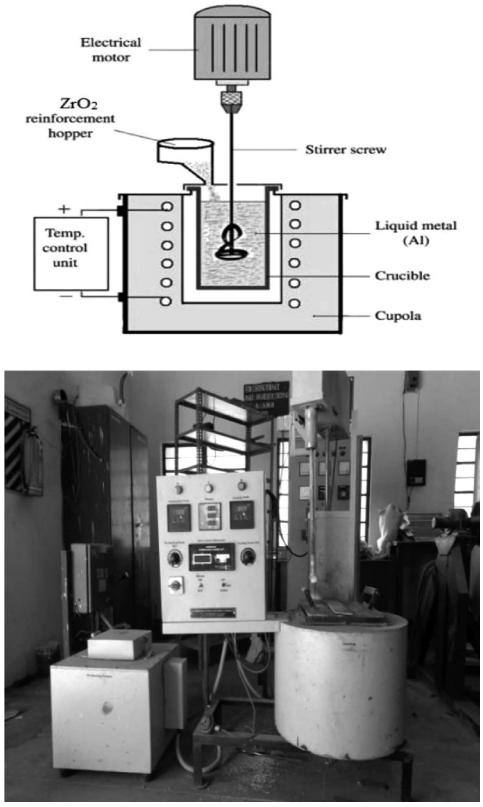


**Figure 1:** a) Schematic view of stir casting setup, casting of MMC by using stir casting method, b) image of stir casting setup, casting of MMC using the stir casting method

**Slika 1:** a) Shematski prikaz sestava za ulivanje z mešanjem, ulivanje MMC z uporabo metode mešanje-ulivanje, posnetek sestava za ulivanje z mešanjem, ulivanje MMC z uporabo metode mešanje-vlivanje

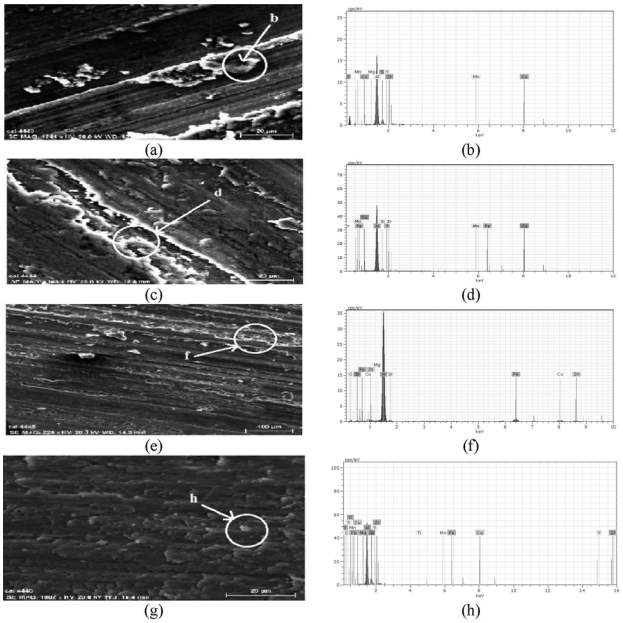


**Figure 2:** SEM images and EDS patterns of various composites: a) SEM image of LM6, b) EDS pattern of LM6, c) SEM image of LM6-3% $ZrO_2$ composites, d) EDS pattern of LM6-3% $ZrO_2$ composites, e) SEM image of LM6-6% $ZrO_2$ Composites, f) EDS pattern of LM6-6% $ZrO_2$ composites, g) SEM image of LM6-9% $ZrO_2$ composites, h) EDS pattern of LM6-9% $ZrO_2$ composites

**Slika 2:** SEM-posnetki in EDS-analiza različnih sestav: a) SEM-posnetek LM6, b) EDS-analiza LM6, c) SEM-posnetek kompozita LM6 – 3 % $ZrO_2$, d) EDS-analiza kompozita LM6 – 3 % $ZrO_2$, e) SEM-posnetek kompozita LM6 – 6 % $ZrO_2$, f) EDS-analiza kompozita LM6 – 6 % $ZrO_2$, g) SEM-posnetek kompozita z 9 % $ZrO_2$, h) EDS-analiza kompozita LM6 – 9 % $ZrO_2$

### *2.2. SEM-EDS analysis of LM6/$ZrO_2$ composite specimen*

Energy-dispersive spectrometry analyses are applied in the present work, which helps to find out information of the type of element present in the samples. From the above **Figures 2b, 2d, 2f** and **2h** indicate the energy-dispersive spectrum of aluminium LM6 with their elements. The **Figures 2a, 2c, 2e** and **2g** indicates the topographical scanning electron microscope (SEM). The microstructure and EDS analysis of $ZrO_2$ particles are shown in **Figures 2e, 2f, 2g** and **2h**. From the graph after finishing EDS test, results are confirmed that the chemical composition of LM6/$ZrO_2$ composites like aluminium, zirconium, iron, copper, magnesium, zinc, silicon, and others all the elements are present in the prepared composites as shown in **Figures 2f** and **2h**. The shrinkage and porosity were not identified in the micrograph. This is evidence of the good quality of the casting. Finally, EDS analyses confirmed the presence of aluminium, $ZrO_2$ particles, which showed in **Figures 2f** and **2h**. The areas or points of the EDS analyses were taken from the SEM images given in **Figures 2a, 2c, 2e** and **2g**.

## 3 RESULTS AND DISCUSSION

### *3.1 Hardness measurements*

Microhardness tests were conducted on the polished samples of aluminium LM6 alloy and its composites by adopting a standard testing procedure. The hardness of the composite was measured using a Vickers microhardness tester as per ASTM: E384-10. All the samples were applied with a load of 300 g for a period of 10 s. The test was carried out at three different locations to avoid the possible effect of the indenter resting on the hard reinforcement particles. The averages of all the five readings were reported. The hardness of the composite depends on the reinforcement of the matrix material. As the coefficient of thermal expansion of zirconia is less than the aluminium alloy, an enormous amount of dislocations are generated at the particle-matrix interface during the solidification process. This makes a further increase in the hardness of the matrix.[5] The results are graphically shown in **Figure 3**. It is observed that the hardness values of the material are directly proportional to the presence of $ZrO_2$, and with the increase in $ZrO_2$, the hardness increases.

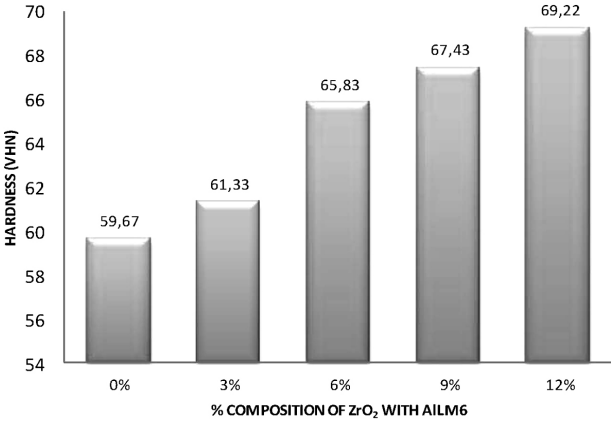


**Figure 3:** Vickers hardness values of various LM6/$ZrO_2$ composites
**Slika 3:** Vrednosti za Vickers trdoto različnih kompozitov LM6/$ZrO_2$


**Figure 4:** Photograph of tensile-tested specimen
**Slika 4:** Posnetek izgleda nateznih preizkušancev

### *3.2 Tensile test*

The 15 tensile test sample specimens were prepared as per the ASTM standard (ASTM B-557-M-94) as shown in **Figure 4**, and they were tested in a Universal Testing Machine (FIE Pvt.Ltd., model: unitek 94100). Before measuring the tensile strength, the 15 samples were machined into a cylindrical shape. Three samples were tested for each composition to obtain the best tensile test result. The tensile tested sample of the five specimens LM6 reinforced with 0 %, 3 %, 6 %, 9 %, and 12 %, respectively, are given in **Figure 4**. From **Figure 5** it is clear that the maximum ultimate tensile strength is obtained for the sample 5, which contains 12 % of $ZrO_2$. Therefore, this clearly reveals that the ultimate tensile strength increases with an increasing percentage of $ZrO_2$, as shown in **Figure 5**. Similar trends have been observed by many other researchers.[6–8]

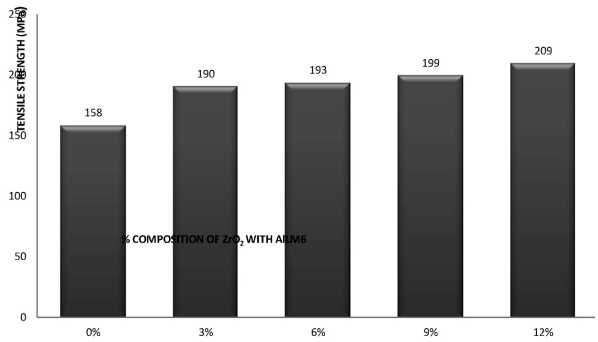


**Figure 5:** Tensile strength of various LM6/$ZrO_2$ composites
**Slika 5:** Natezna trdnost različnih kompozitov LM6/$ZrO_2$

### *3.3 SEM and fractography analysis of tensile specimen*

From these SEM images (**Figures 6** to **8**) it is clear that the distribution of particles throughout the matrix was found to be fairly uniform as a dark region. It is also observed that as the weight percentage of reinforcement of $ZrO_2$ increases the area fraction also increases as shown in **Figures 7** and **8** as a dark region. It can also be noticed that the average grain size of the aluminium LM6 matrix decreases with an increase in the weight fraction of $ZrO_2$ reinforcement.

From these **Figures 7** and **8** it is clear that the homogeneous distributions of $ZrO_2$ reinforced particles with aluminium alloy occurred. Further, these figures reveal the homogeneity of the cast composites. The properties of the aluminium MMCs depend not only on the matrix particle and the weight fraction but also on the distribution of the reinforcing particles and the interface bonding between the particle and the matrix.

Fracture surface analysis revealed different topographies for the composites containing different weight percentages of zirconia particles. The results of the fracture surface analyses conducted on fracture toughness specimens of FCC structured LM6 alloy samples revealed large dimples, along with a large amount of plastic deformation, indicating a ductile fracture. The fracture surfaces also exhibit fine and shallow dimples, indicating that the fracture is ductile, as shown in **Figure 9**.

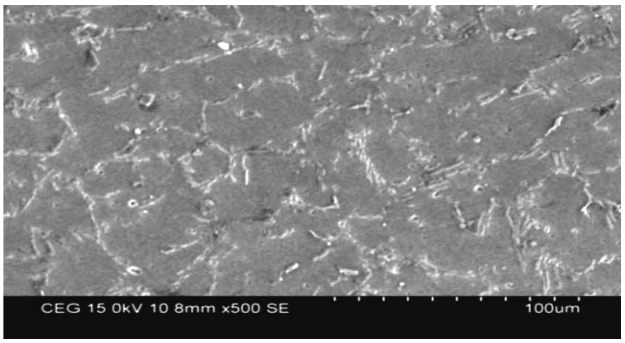


**Figure 6:** SEM image of LM6 alloy
**Slika 6:** SEM-posnetek zlitine LM6


**Figure 7:** SEM image of LM6–6% of $ZrO_2$
**Slika 7:** SEM-posnetek LM6 – 6 % $ZrO_2$

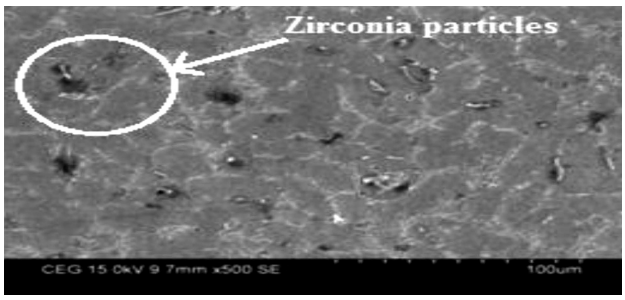


**Figure 8:** SEM image of LM6–12% of $ZrO_2$
**Slika 8:** SEM-posnetek LM6 – 12 % $ZrO_2$

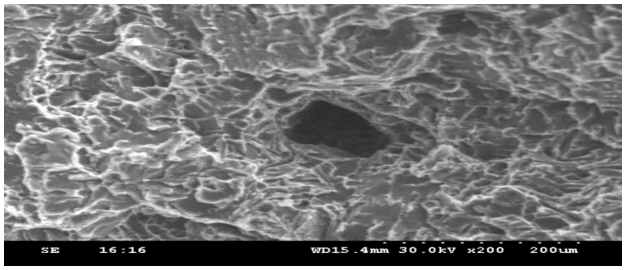


**Figure 9:** Fractured surface of 0% zirconia and 100% LM6
**Slika 9:** Slika preloma pri 0 % $ZrO_2$ in 100 % LM6

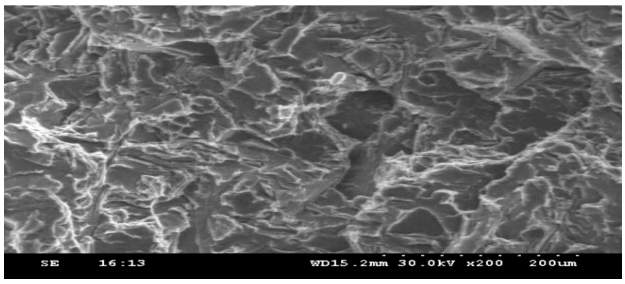


**Figure 10:** Fractured surface of composite with 6 % zirconia and 94 % LM6
**Slika 10:** Površina preloma kompozita z 6 % $ZrO_2$ in 94 % LM6

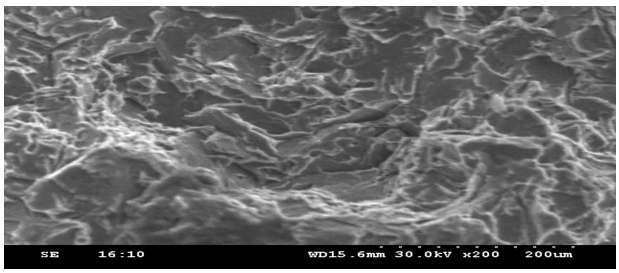


**Figure 11:** Fractured surface of composite with 12 % of zirconia and 88 % LM6
**Slika 11:** Površina preloma kompozita z 12 % $ZrO_2$ in 88 % LM6

Fracture surfaces of the MMCs tested are shown in **Figures 9** to **11**. An examination of these fracture surface features in the SEM at high magnification is to identify the fatigue and final fracture region, to identify areas of micro-crack initiation and early crack growth, and the over-loaded region to identify the fine scale fracture features.

Fracture surfaces revealed different topographies for the composites containing a different weight percentage of zirconia particles. The fracture surface in the case of MMCs containing 12 % of mass fractions reinforcement revealed a cleavage type of fracture (**Figure 11**) due to the presence of excessive zirconia particulates. It can also be seen that regions of clustered particles for reinforcement above 6 % of mass fractions (**Figure 10**) are sensitive to premature damage in the composites and the large particles seem to be prone to fracture and hence registered a reduction in the fracture-toughness value. The fracture mode of the matrix alloy which changed from ductile to cleavage type (in the case of MMCs) was dominated with microcrack nucleation and propagation, as shown in **Figures 9** to **11**. Scanning electron microscope observations of MMCs suggest that, at higher reinforcement content (12 % of mass fractions, **Figure 11**), void nucleation may also take place at large participates in addition to the matrix/particle interface, while at lower reinforcement (0, 6 % of mass fractions, **Figures 9** and **10**) rates the fracture seems to occur through the breakage of the particles.

Fracture surface analysis of MMCs containing 12 % of mass fractions dispersoid (**Figure 11**) exhibit predominantly that fractured particles (dispersoid) and the matrix material with coarse dimples, suggests that fracture is of mixed mode type. Close examination of the fractured surface indicates that most dimples were associated with the matrix material (**Figure 11**). Massive separations of the particle indicate that failure of the material is initiated by the fracture of the particles rather than debonding between the matrix and the reinforcements. The microstructural features are shown in **Figures 10** and **11**, which are a sample containing 12 % of mass fractions dispersion casting of 10 mm thick, which indicates that zirconia particles have fractured during straining and fracture could have occurred in a brittle manner as a result of stress concentrations and the propagation of the cracks. Finally, a composite containing 12 % of mass fractions dispersoid showed cleavage indicating that the fracture is towards brittle.

## 4 CONCLUSIONS

The aluminium-based composite was successfully fabricated by the stir casting method with a uniform distribution of $ZrO_2$ particles.

EDX studies confirmed the presence of aluminium, zirconium, iron, magnesium, silicon in the prepared composite material.

The hardness of the reinforced composites was improved compared with the unreinforced alloy and 12 % of mass fractions of $ZrO_2$ combination achieves the high hardness value.

There is an improvement in the tensile strength, ultimate tensile strength with the addition of $ZrO_2$ particle.

The SEM images of various weight percentage of $ZrO_2$ reinforcement reveal that the SEM image for 12 % of mass fractions of $ZrO_2$ contains more presence of $ZrO_2$ particles. It was clearly seen as a dark region.

The fractography results show that the increase in weight percentage of the $ZrO_2$ changes the mode of failure from ductile to brittle, which is revealed from the occurrence of large dimple tiny particles with a large amount of plastic deformation present in the low weight percentages of $ZrO_2$ reinforced composites.

Fracture surface observation of the samples shows that the failure of the LM6 /zirconia composite is similar to the unreinforced LM6 alloy one, which was controlled by inter-dendrite cracking of the matrix. In addition, a number of dimples were observed on the fracture surface of all the samples, which could be the result of the void nucleation and self-subsequent coalescence during the fracture process.

## 5 REFERENCES

[1] R. Kumar, S. Chauhan, Study on surface roughness measurement for turning of Al 7075/10/SiCp and Al7075 hybrid composites by using Response Surface Methodology and Artificial Neural Networking, Measurement, 65 (**2015**), 166–180, doi:10.1016/j.measurement.2015.01.003

[2] H. J. Choi, S. M. Lee, D. H. Bae, Wear characteristic of aluminum-based composites containing multi-walled carbon nanotubes, Wear, 270 (**2010**), 1–2, 12–18, doi:10.1016/j.wear.2010.08.024

[3] S. Gopalakrishnan, N. Murugan, Production and wear characterization of AA6061 matrix titanium carbide particulate reinforced composite by enhanced stir casting method, Composites Part B: Engineering, 43 (**2012**) 2, 302–308, doi:10.1016/j.compositesb.2011.08.049

[4] M. Hayajneh, A. M. Hassan, A. Alrashdan, A. T. Mayyas, Prediction of tribological of aluminum-copper based composite using Artificial neural network, Journal of Alloys and Compounds, 470 (**2009**) 1–2, 584–588, doi:10.1016/j.jallcom.2008.03.035

[5] S. Das, S. Das, K. Das, Abrasive wear of zircon sand and alumina reinforced Al–4.5 wt% Cu alloy matrix composites—A comparative study, Composites Science and Technology, 67 (**2007**) 3–4, 746–751, doi:10.1016/j.compscitech.2006.05.001

[6] M. Balasubramanian, V. Jayabalan, V. Balasubramanian, Developing mathematical models to predict tensile properties of pulsed current gas tungsten arc welded Ti–6Al–4V alloy, Materials & Design, 29 (**2008**) 1, 92–97, doi:10.1016/j.matdes.2006.12.001

[7] Li Pengting, Li Yunguo, Wu Yuying, Ma Guolong, Liu Xiangfa, Distribution of $TiB_2$ particles and its effect on the mechanical properties of A390 alloy, Materials Science and Engineering: A, 546 (**2012**) 1, 146–152, doi:10.1016/j.msea.2012.03.042

[8] S. C. Tjong, K. C. Lau, Abrasive wear behavior of $TiB_2$ particle-reinforced copper matrix composites, Material Science and Engineering: A, 282 (**2000**) 1–2, 183–186, doi:10.1016/S0921-5093(99)00752-2